Brief Communications

Presynaptic Calcium Channel Inhibition Underlies CB_1 Cannabinoid Receptor-Mediated Suppression of GABA Release

Gergely G. Szabó,[1]* Nora Lenkey,[2]* Noemi Holderith,[2] Tibor Andrási,[1] Zoltan Nusser,[2]† and Norbert Hájos[1]†

[1]Lendület Laboratory of Network Neurophysiology, and [2]Lendület Laboratory of Cellular Neurophysiology, Institute of Experimental Medicine, Hungarian Academy of Sciences, H-1450 Budapest, Hungary

CB_1 cannabinoid receptors (CB_1) are located at axon terminals and effectively control synaptic communication and thereby circuit operation widespread in the CNS. Although it is partially uncovered how CB_1 activation leads to the reduction of synaptic excitation, the mechanisms of the decrease of GABA release upon activation of these cannabinoid receptors remain elusive. To determine the mechanisms underlying the suppression of synaptic transmission by CB_1 at GABAergic synapses, we recorded unitary IPSCs (uIPSCs) at cholecystokinin-expressing interneuron-pyramidal cell connections and imaged presynaptic [Ca^{2+}] transients in mouse hippocampal slices. Our results reveal a power function with an exponent of 2.2 between the amplitude of uIPSCs and intrabouton [Ca^{2+}]. Altering CB_1 function by either increasing endocannabinoid production or removing its tonic activity allowed us to demonstrate that CB_1 controls GABA release by inhibiting Ca^{2+} entry into presynaptic axon terminals via N-type (Cav2.2) Ca^{2+} channels. These results provide evidence for modulation of intrabouton Ca^{2+} influx into GABAergic axon terminals by CB_1, leading to the effective suppression of synaptic inhibition.

Key words: **endocannabinoid; GABAergic interneuron; hippocampus; mouse**

Introduction

G-protein-coupled receptors (GPCRs), one of the largest protein families coded in the genome (Bjarnadóttir et al., 2006), are key regulators of several neuronal functions, including the control of synaptic communication (Hille, 1992). GPCR-dependent regulation of synaptic transmission at axon terminals has been shown to involve the opening of K^+ channels, inhibition of Ca^{2+} channels, blocking vesicle fusion, or the combination of these processes (Miller, 1998; de Jong and Verhage, 2009).

CB_1, one of the most abundant GPCRs in the CNS, is the main receptor of endocannabinoids and the psychoactive ingredient of marihuana (Zimmer et al., 1999; Wilson and Nicoll, 2001). This presynaptic receptor potently affects circuit operation by reducing neurotransmitter release both at excitatory and inhibitory synapses (Kreitzer and Regehr, 2001; Wilson et al., 2001; Brown et al., 2004; Katona and Freund, 2008; Kano et al., 2009). It has been demonstrated that glutamate release is effectively reduced by CB_1 activation in parallel with the suppression of Ca^{2+} influx into cerebellar parallel fiber axon terminals (Kreitzer and Regehr, 2001; Zhang and Linden, 2009). However, the precise mechanism of action is still controversial, because the reduction of Ca^{2+} entry into boutons could be the consequence of either a direct decrease of voltage-gated Ca^{2+} channel function (Brown et al., 2004) or an indirect effect through the opening of presynaptic K^+ channels (Daniel and Crepel, 2001; Daniel et al., 2004). In contrast, the mechanism underlying the reduction of inhibitory synaptic transmission upon CB_1 activation at single-bouton level is still an open question. In this study, we combined electrophysiological recordings with two-photon imaging to address this issue.

Materials and Methods

Slice preparation. CD1 or transgenic mice expressing DsRed fluorescent protein under the control of the cholecystokinin promoter of either sex (postnatal days 16–25) were used (CCK-BAC/DsRedT3 mouse line; Máté et al., 2013). Horizontal hippocampal slices at 250 μm thickness were cut. Animals were anesthetized with isoflurane and decapitated in accordance with the Hungarian Act of Animal Care and Experimentation (1998, XXVIII, Section 243/1998), and with the ethical guidelines of the Institute of Experimental Medicine Protection of Research Subjects Committee. The brains were quickly removed and placed into an ice-cold solution containing the following (in mM): sucrose 204.5, KCl 2.5, $NaHCO_3$ 26, $CaCl_2$ 0.5, $MgCl_2$ 5, NaH_2PO_4 1.25, glucose 10, saturated with 95% O_2 and 5% CO_2, pH 7.2–7.4. Hippocampal slices were prepared using a Leica vibratome (Leica VT1200S; Leica Microsystems), then transferred into an interface-type holding chamber filled with 36°C

Received Jan. 19, 2014; revised April 11, 2014; accepted April 30, 2014.

Author contributions: Z.N. and N. Hajos designed research; G.G.S., N.L., N. Holderith, and T.A. performed research; G.G.S., N.L., N. Holderith, and T.A. analyzed data; G.G.S., N.L., N. Holderith, Z.N., and N. Hajos wrote the paper.

N. Hajos is supported by the National Office for Research and Technology (OMFB-01678/2009). Z.N. is supported by a European Research Council Advanced Grant. Fellowships of the Hungarian Academy of Sciences were awarded to N. Hajos (Lendület, LP2012-23) and Z.N. (Lendület, LP2012-29). We thank Erzsébet Gregori and Dóra Rónaszéki for their excellent technical assistance.

The authors declare no competing financial interests.

*G.G.S. and N.L. contributed equally to this work.

†Z.N. and N. Hajos contributed equally to this work.

Correspondence should be addressed to either Norbert Hájos or Zoltán Nusser, Institute of Experimental Medicine, Hungarian Academy of Sciences, Budapest H-1450, Hungary, E-mail: hajos@koki.hu or nusser@koki.hu.

DOI:10.1523/JNEUROSCI.0247-14.2014

 0270-6474/14/347958-06$15.00/0

aCSF containing the following (in mM): NaCl 126, KCl 2.5, $NaHCO_3$ 26, $CaCl_2$ 2, $MgCl_2$ 2, NaH_2PO_4 1.25, glucose 10, saturated with 95% O_2 and 5% CO_2, pH 7.2–7.4. Slices were kept up to 6 h in the holding chamber before recordings. The same solutions were used during electrophysiological and two-photon imaging experiments.

Electrophysiological recordings. Slices were transferred to a submerged recording chamber. The flow rate was 2–3 ml/min. Experiments were performed at room temperature under visual guidance. For electrophysiological recordings, an Olympus microscope (BX61WI) was used equipped with a monochromator. DsRed in cells was excited at 488 nm wavelength, and the resulting fluorescence was detected with a CCD camera (TILL Photonics). Whole-cell patch-clamp recordings were made using a Multiclamp 700B amplifier (Molecular Devices), traces were filtered at 3 kHz, digitized at 10 kHz with a PCI-6024E board (National Instruments), recorded with an in-house data acquisition and stimulation software, and off-line analyzed using EVAN software (courtesy of Istvan Mody, Department of Neurology, UCLA). Patch pipettes were pulled (Zeitz Universal Puller, Zeitz-Instrumente Vertriebs) from thin-walled borosilicate glass capillaries with an inner filament (1.5 mm outer diameter, 1.17 mm inner diameter; Harvard Apparatus). Pipette resistance was 5–7 MΩ when filled with the intrapipette solution. For recording interneurons the intrapipette solution contained the following (in mM): K-gluconate 130, KCl 5, $MgCl_2$ 2, creatine phosphate 10, HEPES 10, Na_2ATP 2, Na_2GTP 1, and biocytin, 7. The solution also contained 100 μM Fluo-5F (Invitrogen, $K_D \sim 2.3$ μM). The pH was adjusted to 7.3, the osmolarity was 290–300 mOsm. Interneurons were held between −60 and −65 mV (with 0 to −250 pA DC current injections) and pairs of action potentials (APs) at 10 Hz were evoked in every 30 s with 1.5–2 ms long depolarizing (1–1.2 nA) current pulses. Presynaptic interneurons were selected based on their DsRed content. The interneurons were sampled from strata pyramidale, lucidum, and radiatum. The physiological characteristics of interneurons were determined from their voltage responses to series of hyper- and depolarizing square current pulses of 800 ms duration and amplitudes ranging from −100 to 100 pA with 10 pA increments and to 500 pA with 50 pA increments. Intrapipette solution used for the postsynaptic cell contained (in mM) 80 CsCl, 60 Cs-gluconate, 1 $MgCl_2$, 2 Mg-ATP, 3 NaCl, 10 HEPES, 5 QX-314 [2(triethylamino)-*N*-(2,6-dimethylphenyl) acetamine] and 25 μM AlexaFluor 488, adjusted to pH 7.3 with CsOH. The osmolarity of the solution was 295 mOsm. Unitary IPSCs (uIPSCs) were recorded in monosynaptically connected pyramidal cells that were voltage-clamped at the holding potential of −65 mV. Series resistance was frequently monitored and 65% compensation was applied. In paired recordings, similarly to the imaging experiments, we waited 1 h to equilibrate the intrapipette solution within the cells. During this period, we obtained a stable recording in a connected pyramidal cell. After 1 h, 40 uIPSCs were recorded as a control period within 20 min, followed by the drug application. Drugs were applied for 35 or 50 min and the values obtained during the last 20 min were used to compare with the values recorded in control conditions. In addition, we performed control experiments in which either BSA or aCSF was applied without any drug to reveal the magnitude of the "rundown" during our experimental conditions. These control experiments were randomly distributed throughout the whole experiment series and showed similar amplitude distribution and similar extent of change in series resistance. Control experiments using DMSO were performed in one block. On average, we found a rundown of 17.9 ± 13.2% ($n = 8$) in control experiments for ω-Conotoxin GVIA (ω-CTx) treatment, 15.3 ± 35% ($n = 4$) in controls for AM251 application, and 8.3 ± 3.6% ($n = 8$) in controls for carbachol (CCh) treatment, which was used to correct the effects of drugs. DMSO applied at 0.01% caused a nonsignificant change in the IPSC amplitude (11.4 ± 11.2%, $n = 4$; $p = 0.26$, paired *t* test). In addition, all experiments that showed >50% rundown during the control period (i.e., in the first 20 min) were discarded.

Two-photon imaging. For imaging experiments, the same stimulus and experimental protocol was applied as in the electrophysiological recordings. Recording solutions were also identical, except that intrapipette solution for imaging experiments contained 25 μM AlexaFluor 594 (Invitrogen). Cells were visualized in slices using a Femto2D microscope (Femtonics) equipped with oblique infrared illumination and a water-immersion lens (25×, 1.05 NA, Olympus). Whole-cell recordings from cholecystokinin (CCK)-immunopositive interneurons were performed in current-clamp mode using a MultiClamp 700A amplifier. Electrophysiological traces were filtered at 3 kHz and digitized on-line at 20 kHz. Drugs were applied using a recirculation system with a peristaltic pump, where the total volume was ~6 ml and the solutions were equilibrated with 95% O_2 and 5% CO_2. Two-photon imaging experiments were performed with a Femto2D laser-scanning microscope, using a MaiTai femtosecond pulsing laser (SpectraPhysics) tuned to 810 nm. A detailed description of the setup and calculation of G/G_{max} values was described previously (Holderith et al., 2012). Bouton-strings at 20–60 μm depth in the tissue and usually between 150 and 300 μm from the soma were selected preferentially at or near the stratum pyramidale in the CA3 region. There was no correlation between the distance of the bouton-string from the soma and (1) the peak $[Ca^{2+}]_i$, (2) decay of $[Ca^{2+}]_i$ transients, and (3) amplitude and SD of the AlexaFluor 594 fluorescent signal. After 1 h loading period, a 20 min "control" scanning period was performed during which ~10–15 boutons were scanned each two times separated by 30 s. The same 20 min scanning period was repeated on the same boutons after a 15 (for AM251, CCh, or 1 μM ω-Conotoxin GVIA; ω-CTx) or a 30 (for 1–50 nM ω-CTx) min drug equilibration period. Transients derived from the two sequential scans were averaged for each bouton. The recorded $[Ca^{2+}]_i$ transients were considered to originate from boutons, if the $[Ca^{2+}]_i$ transient following filtering at 50 Hz reached the peak within 18 ms after the action potential, and the signal increased monotonically. If they passed this test, the peak of $[Ca^{2+}]_i$ transients was determined with 200 Hz filtering and the largest value within a time window of 2–8 ms after the action potential was used. The amplitude of $[Ca^{2+}]_i$ transients went through a gradual decline during the ~1 h of imaging session in aCSF, therefore all drug effects were normalized to their corresponding reduction obtained in aCSF. These reductions controlling 1 μM ω-CTx, 1–50 nM ω-CTx, 1–2 μM AM251, and CCh, were 18.4 ± 4.7%, 16.3 ± 4.4%, 10.5 ± 14.1%, and 10.5 ± 14.1%, respectively. All data are normalized with these values except raw traces. Control experiments were performed to show that 1 mg/ml BSA together with 0.1% DMSO has no effect on the amplitude of the $[Ca^{2+}]_i$ transients ($p = 0.27$, paired *t* test). The 16.0 ± 10.4% reduction of the peak $[Ca^{2+}]_i$ in these experiments was similar to the 9.3 ± 15.4% decrement that was obtained in aCSF controls ($p = 0.62$, unpaired *t* test). The basal $[Ca^{2+}]_i$ level was also monitored before action potential initiations. During drug applications the basal $[Ca^{2+}]_i$ levels were reduced by 8.8 ± 46.4%, 12.0 ± 22.9% and 23.5 ± 29.4% in aCSF, AM251 and CCh, respectively. There was no significant difference in either the basal $[Ca^{2+}]_i$ level ($p = 0.18$, ANOVA) or the change of it among different experimental conditions (aCSF/AM251/CCh application, $p = 0.41$, ANOVA). The effects of AM251 and CCh did not depend on the basal $[Ca^{2+}]_i$ level or the change of the basal $[Ca^{2+}]_i$ level of boutons ($p > 0.3$ for all Pearson correlations).

Immunohistochemistry. After recordings, slices were fixed in a fixative containing 4% paraformaldehyde, 0.2% picric acid in 0.1 M phosphate buffer (PB; pH 7.4) at 4°C at least for 12 h. Following the fixation, the slices were washed in PB several times, embedded in agarose (2%) and resectioned at 50–80 μm thickness. Sections were washed with PB and blocked in normal goat serum (10%), made up in Tris-buffered saline (TBS; pH = 7.4). CB_1 was visualized using a rabbit or a guinea pig anti-CB_1 antibody (1:1000; Cayman Chemicals and Frontier Institute, respectively) diluted in TBS containing 0.1% Triton X-100. Following several washes in TBS, AlexaFluor 488-conjugated goat anti-rabbit IgG (1:500; Jackson ImmunoResearch) or Dylight405-conjugated goat anti-guinea pig (1:500, Jackson ImmunoResearch) was used to visualize the CB_1 immunoreaction, while Cy3-conjugated streptavidin (1:500–1:3000; Invitrogen) was used to visualize the biocytin. Sections were then mounted on slides in Vectashield (Vector Laboratories). Images were acquired using Olympus FV1000 confocal microscope with either a 20× or a 60× oil-immersion objective or with an AxioImager.Z1 using 40× objective (Zeiss). Cells identified as basket or mossy fiber-associated interneurons based on their axonal arborizations were included in the analysis (Gulyás et al., 1993; Losonczy et al., 2004). Only CB_1-immunopositive interneurons were included in the study. Subsequently, some cells were further

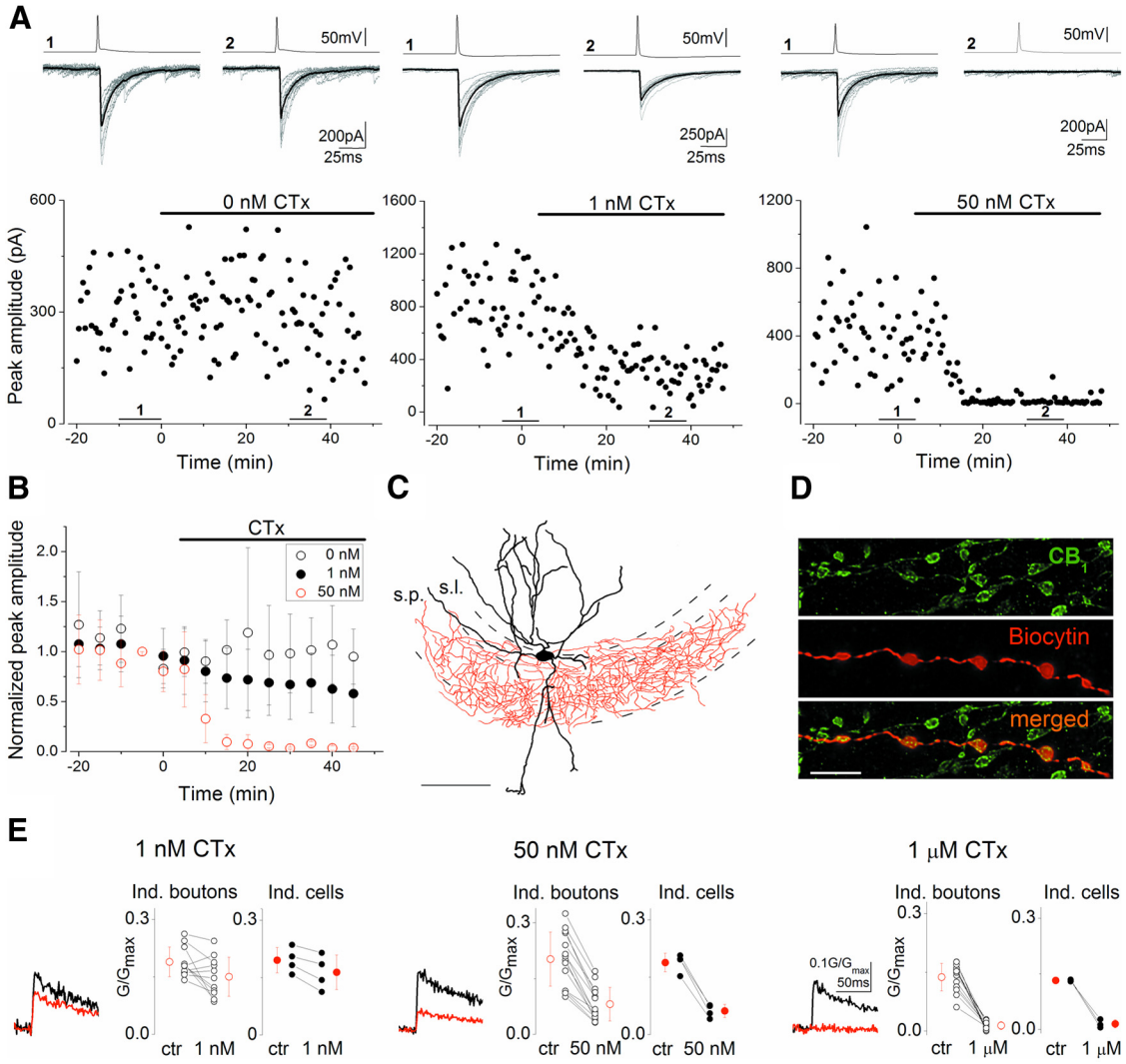

Figure 1. The N-type voltage-gated Ca^{2+} channel blocker, ω-CTx suppresses both uIPSC amplitudes evoked by CB_1-expressing interneurons in CA3 PCs and presynaptic $[Ca^{2+}]$ transients in a dose-dependent manner. Experiments were performed in the presence of the CB_1 antagonist, AM251 (1 μM). ***A***, Representative experiments showing the changes in uIPSC amplitudes under control conditions and upon bath application of 1 or 50 nM ω-CTx. Presynaptic action potentials (top traces) and concomitantly recorded uIPSCs (bottom traces; 10 individuals, gray; averages, black) are shown. Numbers 1 and 2 indicate the period where traces from control and drug conditions were selected, respectively. ***B***, Summary plots of normalized uIPSC amplitudes at three different conditions. Error bars represent SD. The effect of 1 and 50 nM ω-CTx are statistically significant (paired *t* test, $p < 0.05$). ***C***, Reconstruction of a representative CB_1-immunolabeled basket cell (dendrites, black; axons, red; s.p., stratum pyramidale; s.l., stratum lucidum). Scale bar, 100 μm. ***D***, A biocytin-filled axon of a presynaptic interneuron is immunopositive for CB_1. Scale bar, 5 μm. ***E***, Averages of 14–20 $[Ca^{2+}]_i$ transients measured at 7–10 boutons in a single cell in control conditions (black traces) and in the presence of 1 and 50 nM and 1 μM ω-CTx (red traces). Scale bars on the right refer to each trace. Open symbols represent the amplitude of $[Ca^{2+}]_i$ transients recorded from individual boutons of a representative cell. Filled symbols represent the mean of individual cells. All drug effects are statistically significant both at individual bouton levels and for individual cells (paired *t* test, $p < 0.05$). Mean ± SD are shown in red.

developed by immunoperoxidase reaction (ABC; Vector Laboratories) using 3–3-diaminobenzidine tetrahydrochloride together with ammonium nickel sulfate hexahydrate ($(NH_4)_2(NiSO_4)_2{\cdot}6H_2O$) (DAB-Ni) as a chromogen. After dehydration and embedding in Durcupan, representative cells were reconstructed with the aid of a drawing tube using a 40× objective.

Drugs. ω-CTx (Tocris Bioscience, product no. 1085) stock was dissolved in distilled water and diluted to a final concentration in aCSF together with 1 mg/ml BSA. AM251 (Tocris Bioscience, product no. 1117) was dissolved in DMSO to reach 10 mM stock solution, CCh (20 mM stock) was dissolved in distilled water. All drugs were purchased from Sigma-Aldrich unless indicated otherwise.

Data analysis and statistical tests. Two-photon imaging data and partly the electrophysiological data were analyzed using MES (Femtonics). Data were plotted using Origin 8.6 software. Statistical significance of the drug effect was assessed with Student's paired *t* test for experiments using ω-CTx and Wilcoxon signed rank test for experiments applying AM251 or CCh. Results were considered significant at $p < 0.05$. Data are presented as mean ± SD unless indicated otherwise.

Calculation of the $[Ca^{2+}]_i$–uIPSC relationship curve. First, dose–response curves for ω-CTx were determined on $[Ca^{2+}]_i$ transients and uIPSCs. The tested drug concentrations were 0.1, 1, 10, and 50 nM for uIPSCs, and 1, 10, 50, and 1000 nM for $[Ca^{2+}]_i$ transients. Throughout these experiments, 1 μM AM251 was applied to avoid differential tonic CB1 activation. By fitting the dose–response curves with a sigmoidal function ($f(x) = 1/(1 + (x/x_0)^p)$), the effect of 1 μM ω-CTx on uIPSCs and 0.1 nM ω-CTx on $[Ca^{2+}]_i$ transients could be estimated. Incorporating these two values into the measured dataset, a $[Ca^{2+}]_i$–uIPSC relationship curve was constructed (see Fig. 2*M*). Each point corresponds to a given ω-CTx concentration (from left to right: 1000, 50, 10, 1, and 0.1 nM). Red data point shows the effect of tonic CB_1 activity that is the inverse of the AM251 effect. In other words, it corresponds to uIPSCs amplitude and peak $[Ca^{2+}]_i$ transients in control condition, from which AM251 application enhanced the amplitudes to the 1:1 data point. We calculated this point by taking the effects of AM251 in individual cells, took their reciprocal values and calculated the average and SEM. Blue

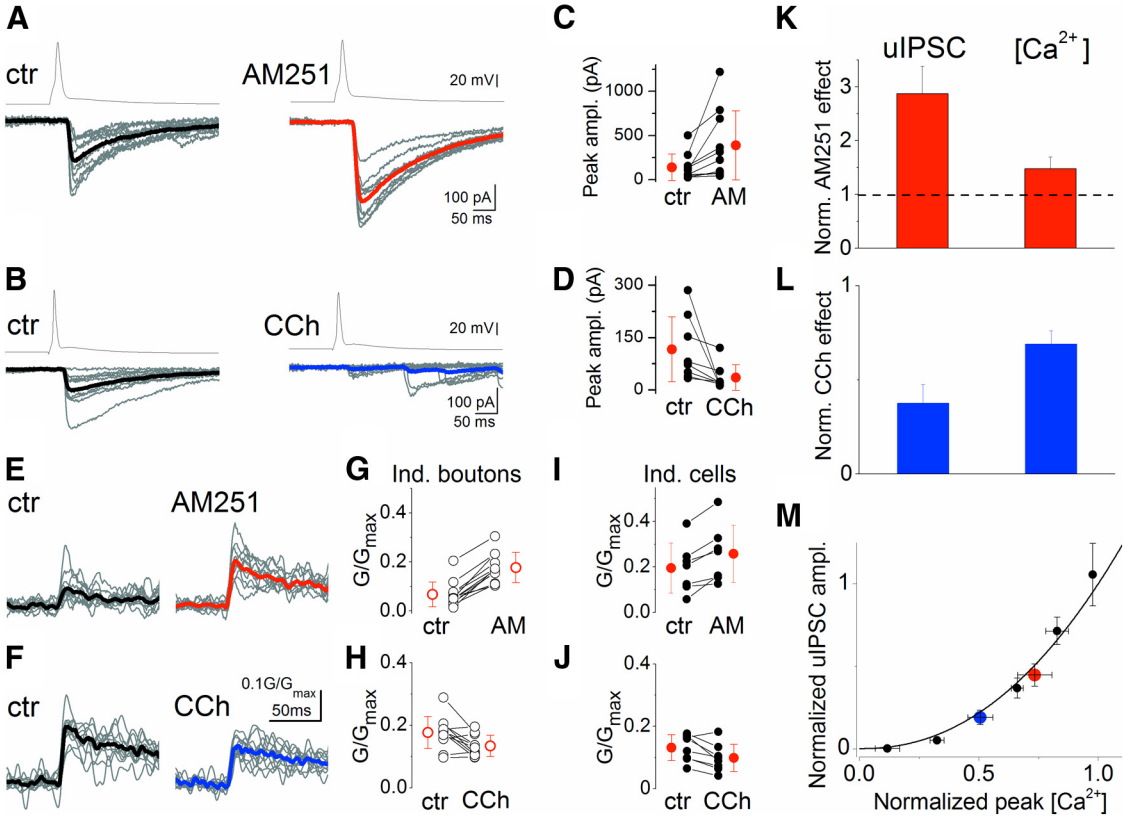

Figure 2. CB_1 activation controls the amplitude of uIPSCs by altering presynaptic $[Ca^{2+}]_i$ transients. ***A***, AM251 (1 μM) application increases uIPSC amplitudes. ***B***, Muscarinic receptor activation by CCh (5 μM), which triggers endocannabinoid synthesis, results in a robust reduction in uIPSC amplitudes. ***C***, ***D***, Summary plots of the effects of AM251 and CCh on uIPSC peak amplitudes (changes were significant; Wilcoxon signed rank test, $p < 0.01$). ***E–J***, AM251 and CCh have opposite effects on the amplitude of presynaptic $[Ca^{2+}]_i$ transients both at the levels of individual boutons (***E***, ***H***), and of individual cells (***I***, ***J***). Mean ± SD is shown in red. The effects were statistically significant (Wilcoxon signed rank test, $p < 0.05$). ***K***, ***L***, Normalized values of the drug effects on peak uIPSC amplitudes and on $[Ca^{2+}]_i$ transients observed in AM251 and CCh. Mean ± SEM are shown. ***M***, Relationship between normalized $[Ca^{2+}]_i$ and uIPSC amplitude at different ω-CTx concentrations (black; 1 μM, 50 nM, 10 nM, 1 nM, and 0.1 nM data points from left to right) is shown and superimposed are the effects of CCh (blue) and tonic CB_1 activation (inverse of AM251 effect: red; see Materials and Methods). The curve was fitted by power function ($f(x) = x^m$) with an m of 2.2. Error bars represent SEM.

symbol represents the effect of CCh normalized to control condition (to the red point).

The relationship between $[Ca^{2+}]_i$ and uIPSC was estimated by fitting it with a power function ($f(x) = x^m$) using dataset from ω-CTx experiments. Fitting the recorded data gave an exponent $m = 2.2$. We performed bootstrap analysis to validate that our experimental dataset size was large enough for correct estimation of the fit, and calculate confidence intervals. Bootstrap analysis resulted in an m value of 2.2 ± 0.4. Data points regarding CCh and AM251 application (see Fig. 2*M*, blue and red symbols) fell inside the confidence intervals, therefore CCh and AM251 effect were considered not significantly different from Ca^{2+} channel blocking effect of ω-CTx.

Results

Here, we aimed to uncover how CB_1 activation leads to the suppression of GABAergic transmission in the hippocampus. As a first step, we determined the relationship between action potential-evoked $[Ca^{2+}]$ transients in axon terminals ($[Ca^{2+}]_i$) of CCK and CB_1-expressing perisomatic targeting interneurons (basket and mossy fiber-associated cells) and the amplitude of uIPSCs (Bucurenciu et al., 2010) recorded in CA3 pyramidal cells (PCs). To eliminate the possible effects of differential tonic CB_1 activation in slices, a CB_1 antagonist (AM251, 1 μM) was continuously applied. Bath application of ω-CTx (a Cav2.2/N-type calcium channel inhibitor) at different concentrations decreased the uIPSC amplitudes (Wilson et al., 2001) in a dose-dependent manner and fully blocked the postsynaptic response at concentrations >50 nM (Fig. 1*A–D*). In a separate set of experiments, ω-CTx dose-dependently reduced $[Ca^{2+}]_i$ transients evoked by single action potentials (Fig. 1*E*). Importantly, 1 μM ω-CTx completely eliminated the $[Ca^{2+}]_i$ transients, demonstrating that action potential-evoked Ca^{2+} entry into CB_1-immunopositive boutons is mainly, if not exclusively conducted via N-type Ca^{2+} channels.

To reveal the relationship between Ca^{2+} entry and subsequent transmitter release, we plotted the normalized uIPSC amplitudes as a function of normalized peak $[Ca^{2+}]_i$ obtained in paired recordings and presynaptic Ca^{2+} imaging, respectively (Fig. 2). The plot was fitted with a power function with an exponent of 2.2 (Fig. 2*M*), showing that a supralinear cooperativity of Ca^{2+} controls the GABA release from CCK+ axon terminals.

Next, we sought to reveal the mechanisms underlying the suppression of inhibitory synaptic transmission by CB_1. If CB_1 activation reduces IPSC amplitude solely via the inhibition of Ca^{2+} entry, altering CB_1 function should result in changes in the corresponding $[Ca^{2+}]_i$ and uIPSC values in a way that they ought to fall onto the $[Ca^{2+}]_i$-uIPSC curve derived from the ω-CTx experiments. Alternatively, if these changes do not follow the $[Ca^{2+}]_i$-uIPSC relationship, additional mechanisms must play a role. To address this issue, first we examined the effect of tonic CB_1 activation on uIPSCs. AM251 (1–2 μM) application increased the peak amplitude of uIPSCs in individual pairs to dif-

ferent extents (Fig. 2*A*,*C*), suggesting that there is a differential tonic activation of the CB_1 at these inhibitory synapses. Next, the synthesis of endocannabinoids was augmented by bath application of an acetylcholine receptor agonist (CCh; 5 μM; Kim et al., 2002; Makara et al., 2007). The drug treatment resulted in a significant reduction in the peak amplitude of the uIPSCs (Fig. 2*B*,*D*), an effect that has been shown to be mediated via CB_1 in the CA3 region (Szabó et al., 2010). In parallel experiments, action potential-evoked $[Ca^{2+}]_i$ transients were augmented by AM251 and suppressed by CCh (Fig. 2*E–J*). Both AM251 and CCh caused a more robust change in the uIPSC amplitudes than in $[Ca^{2+}]_i$ (Fig. 2*K*,*L*). When we calculated the normalized changes in uIPSC amplitudes and $[Ca^{2+}]_i$, we found that the obtained data points fell on the $[Ca^{2+}]_i$-uIPSC curve (Fig. 2*M*). These results indicate that CB_1 activation reduces GABA release by suppressing the Ca^{2+} entry into presynaptic boutons via inhibition of N-type voltage-gated Ca^{2+} channel function.

Discussion

We have examined the cellular mechanisms underlying the suppression of inhibitory synaptic transmission upon CB_1 activation in the CA3 region of acute hippocampal slices. Our principal findings are as follows: (1) N-type voltage-gated Ca^{2+} channels are the main, if not the only source of the action potential-evoked Ca^{2+} entry into the boutons expressing CB_1. (2) There is a supralinear cooperativity of intraboutonal $[Ca^{2+}]$ and the GABA release at CCK/CB_1-positive GABAergic synapses. (3) CB_1 cannabinoid receptors suppress GABA release via inhibition of N-type voltage-gated Ca^{2+} channel function.

Our measurements demonstrated that N-type voltage-gated Ca^{2+} channels mediated mainly, if not exclusively the action potential-evoked Ca^{2+} entry into GABAergic boutons expressing CCK/CB_1, in line with the previously proposed hypothesis (Wilson et al., 2001; Hefft and Jonas, 2005). Although Ca^{2+} release from intracellular Ca^{2+} stores could contribute to the volume-averaged $[Ca^{2+}]_i$ transients, as shown at cerebellar inhibitory synapses (Llano et al., 2000), its magnitude may be low at stimulus frequencies used in the present study (Carter et al., 2002). In addition, spontaneous opening of N-type Ca^{2+} channels at CB_1-expressing axon terminals can contribute also to the action potential-independent GABA release (Goswami et al., 2012), which could play a role in stabilizing synaptic function (Farrant and Nusser, 2005).

Similar to other central synapses (von Gersdorff et al., 1998; Fedchyshyn and Wang, 2005; Bucurenciu et al., 2010), at CCK-expressing inhibitory perisomatic synapses the cooperativity of Ca^{2+} is supralinear, even though the GABA release is not as tightly coupled to the opening of presynaptic Ca^{2+} channels as in parvalbumin-containing GABAergic axon terminals (Hefft and Jonas, 2005; Bucurenciu et al., 2008). The obtained power coefficient of 2.2 is somewhat greater than those determined for the relationship between the presynaptic $[Ca^{2+}]$ and the magnitude of postsynaptic responses at parvalbumin-expressing inhibitory synapses in the dentate gyrus (1.6) or at both auditory hair cell and retinal ribbon synapses (1.1–1.4), but lower than that determined at young calyx of Held synapses (>3; Eggermann et al., 2012). Because N-type Ca^{2+} channels are activated with high efficacy by action potentials (Li et al., 2007), only a relatively small number of channels located near the active zone should be responsible for presynaptic Ca^{2+} influx evoking GABA release at CCK/CB1-expressing synapses (Eggermann et al., 2012).

We clarified that inhibition of N-type Ca^{2+} channel function is the main, if not the sole mechanism underlying the CB_1-mediated suppression of synaptic inhibition, which is in line with a previous proposal based on data obtained in cell lines (Mackie and Hille, 1992). By uncovering the detailed mechanisms of how presynaptically located CB_1 regulates transmitter release, we open up new avenues leading to a better understanding how endocannabinoids and ^{9d}THC exert their influence on the CNS.

References

Bjarnadóttir TK, Gloriam DE, Hellstrand SH, Kristiansson H, Fredriksson R, Schiöth HB (2006) Comprehensive repertoire and phylogenetic analysis of the G-protein-coupled receptors in human and mouse. Genomics 88:263–273. CrossRef Medline

Brown SP, Safo PK, Regehr WG (2004) Endocannabinoids inhibit transmission at granule cell to Purkinje cell synapses by modulating three types of presynaptic calcium channels. J Neurosci 24:5623–5631. CrossRef Medline

Bucurenciu I, Kulik A, Schwaller B, Frotscher M, Jonas P (2008) Nanodomain coupling between Ca2+ channels and Ca2+ sensors promotes fast and efficient transmitter release at a cortical GABAergic synapse. Neuron 57:536–545. CrossRef Medline

Bucurenciu I, Bischofberger J, Jonas P (2010) A small number of open Ca2+ channels trigger transmitter release at a central GABAergic synapse. Nat Neurosci 13:19–21. CrossRef Medline

Carter AG, Vogt KE, Foster KA, Regehr WG (2002) Assessing the role of calcium-induced calcium release in short-term presynaptic plasticity at excitatory central synapses. J Neurosci 22:21–28. Medline

Daniel H, Crepel F (2001) Control of Ca(2+) influx by cannabinoid and metabotropic glutamate receptors in rat cerebellar cortex requires K(+) channels. J Physiol 537:793–800. CrossRef Medline

Daniel H, Rancillac A, Crepel F (2004) Mechanisms underlying cannabinoid inhibition of presynaptic Ca2+ influx at parallel fibre synapses of the rat cerebellum. J Physiol 557:159–174. CrossRef Medline

de Jong AP, Verhage M (2009) Presynaptic signal transduction pathways that modulate synaptic transmission. Curr Opin Neurobiol 19:245–253. CrossRef Medline

Eggermann E, Bucurenciu I, Goswami SP, Jonas P (2012) Nanodomain coupling between Ca(2+) channels and sensors of exocytosis at fast mammalian synapses. Nat Rev Neurosci 13:7–21. CrossRef Medline

Farrant M, Nusser Z (2005) Variations on an inhibitory theme: phasic and tonic activation of GABA(A) receptors. Nat Rev Neurosci 6:215–229. CrossRef Medline

Fedchyshyn MJ, Wang LY (2005) Developmental transformation of the release modality at the calyx of Held synapse. J Neurosci 25:4131–4140. CrossRef Medline

Goswami SP, Bucurenciu I, Jonas P (2012) Miniature IPSCs in hippocampal granule cells are triggered by voltage-gated Ca2+ channels via microdomain coupling. J Neurosci 32:14294–14304. CrossRef Medline

Gulyás AI, Miles R, Hájos N, Freund TF (1993) Precision and variability in postsynaptic target selection of inhibitory cells in the hippocampal CA3 region. Eur J Neurosci 5:1729–1751. CrossRef Medline

Hefft S, Jonas P (2005) Asynchronous GABA release generates long-lasting inhibition at a hippocampal interneuron-principal neuron synapse. Nat Neurosci 8:1319–1328. CrossRef Medline

Hille B (1992) G-protein-coupled mechanisms and nervous signaling. Neuron 9:187–195. Medline

Holderith N, Lorincz A, Katona G, Rózsa B, Kulik A, Watanabe M, Nusser Z (2012) Release probability of hippocampal glutamatergic terminals scales with the size of the active zone. Nat Neurosci 15:988–997. CrossRef Medline

Kano M, Ohno-Shosaku T, Hashimotodani Y, Uchigashima M, Watanabe M (2009) Endocannabinoid-mediated control of synaptic transmission. Physiol Rev 89:309–380. CrossRef Medline

Katona I, Freund TF (2008) Endocannabinoid signaling as a synaptic circuit breaker in neurological disease. Nat Med 14:923–930. CrossRef Medline

Kim J, Isokawa M, Ledent C, Alger BE (2002) Activation of muscarinic acetylcholine receptors enhances the release of endogenous cannabinoids in the hippocampus. J Neurosci 22:10182–10191. Medline

Kreitzer AC, Regehr WG (2001) Retrograde inhibition of presynaptic calcium influx by endogenous cannabinoids at excitatory synapses onto Purkinje cells. Neuron 29:717–727. CrossRef Medline

Li L, Bischofberger J, Jonas P (2007) Differential gating and recruitment of

P/Q-, N-, and R-type Ca2+ channels in hippocampal mossy fiber boutons. J Neurosci 27:13420–13429. CrossRef Medline

Llano I, González J, Caputo C, Lai FA, Blayney LM, Tan YP, Marty A (2000) Presynaptic calcium stores underlie large-amplitude miniature IPSCs and spontaneous calcium transients. Nat Neurosci 3:1256–1265. CrossRef Medline

Losonczy A, Biró AA, Nusser Z (2004) Persistently active cannabinoid receptors mute a subpopulation of hippocampal interneurons. Proc Natl Acad Sci U S A 101:1362–1367. CrossRef Medline

Mackie K, Hille B (1992) Cannabinoids inhibit N-type calcium channels in neuroblastoma-glioma cells. Proc Natl Acad Sci U S A 89:3825–3829. CrossRef Medline

Makara JK, Katona I, Nyíri G, Németh B, Ledent C, Watanabe M, de Vente J, Freund TF, Hájos N (2007) Involvement of nitric oxide in depolarization-induced suppression of inhibition in hippocampal pyramidal cells during activation of cholinergic receptors. J Neurosci 27:10211–10222. CrossRef Medline

Máté Z, Poles MZ, Szabó G, Bagyánszki M, Talapka P, Fekete E, Bódi N (2013) Spatiotemporal expression pattern of DsRedT3/CCK gene construct during postnatal development of myenteric plexus in transgenic mice. Cell Tissue Res 352:199–206. CrossRef Medline

Miller RJ (1998) Presynaptic receptors. Annu Rev Pharmacol Toxicol 38:201–227. CrossRef Medline

Szabó GG, Holderith N, Gulyás AI, Freund TF, Hájos N (2010) Distinct synaptic properties of perisomatic inhibitory cell types and their different modulation by cholinergic receptor activation in the CA3 region of the mouse hippocampus. Eur J Neurosci 31:2234–2246. CrossRef Medline

von Gersdorff H, Sakaba T, Berglund K, Tachibana M (1998) Submillisecond kinetics of glutamate release from a sensory synapse. Neuron 21:1177–1188. CrossRef Medline

Wilson RI, Nicoll RA (2001) Endogenous cannabinoids mediate retrograde signalling at hippocampal synapses. Nature 410:588–592. CrossRef Medline

Wilson RI, Kunos G, Nicoll RA (2001) Presynaptic specificity of endocannabinoid signaling in the hippocampus. Neuron 31:453–462. CrossRef Medline

Zhang W, Linden DJ (2009) Neuromodulation at single presynaptic boutons of cerebellar parallel fibers is determined by bouton size and basal action potential-evoked Ca transient amplitude. J Neurosci 29:15586–15594. CrossRef Medline

Zimmer A, Zimmer AM, Hohmann AG, Herkenham M, Bonner TI (1999) Increased mortality, hypoactivity, and hypoalgesia in cannabinoid CB1 receptor knock-out mice. Proc Natl Acad Sci U S A 96:5780–5785. CrossRef Medline